Excitation of stable Alfvén eigenmodes by application of alternating magnetic field perturbations in the Compact Helical System

T. Ito,[1] K. Toi,[2] G. Matsunaga,[3] M. Isobe,[2] K. Nagaoka,[2] M. Takeuchi,[2] T. Akiyama,[2] K. Matsuoka,[2] T. Minami,[2] S. Nishimura,[2] S. Okamura,[2] A. Shimizu,[2] C. Suzuki,[2] Y. Yoshimura,[2] C. Takahashi,[2] and CHS Experimental Group
[1]*Department of Energy Engineering and Science, Nagoya University, Nagoya, Aichi 464-8601, Japan*
[2]*National Institute for Fusion Science, Toki, Gifu 509-5292, Japan*
[3]*Japan Atomic Energy Agency, Naka, Ibaraki 311-0193, Japan*

(Received 27 April 2009; accepted 17 August 2009; published online 14 September 2009)

Stable toroidicity-induced Alfvén eigenmodes (TAEs) with low toroidal mode number ($n=1$ and $n=2$) were excited by application of alternating magnetic field perturbations generated with a set of electrodes inserted into the edge region of neutral beam injection heated plasmas on the Compact Helical System [K. Nishimura, K. Matsuoka, M. Fujiwara *et al.*, Fusion Technol. **17**, 86 (1990)]. The gap locations of TAEs excited by the electrodes are in the plasma peripheral region of $\rho>0.7$ (ρ is the normalized minor radius) where energetic ion drive is negligibly small, while some AEs are excited by energetic ions in the plasma core region of $\rho<0.4$. The damping rate of these stable TAEs derived from plasma responses to applied perturbations is fairly large, that is, ~9% to ~12% of the angular eigenfrequency. This large damping rate is thought to be dominantly caused by continuum damping and radiative damping. © *2009 American Institute of Physics*.
[doi:10.1063/1.3223845]

I. INTRODUCTION

In a burning plasma, large amplitude magnetohydrodynamic (MHD) instabilities such as Alfvén eigenmodes (AEs) excited by resonant interaction with fusion-born alpha particles would enhance radial transport and/or loss of these alphas. It is concerned that enhanced loss of alphas would lead to serious damage of plasma facing components.[1] Especially, toroidicity-induced AEs (TAEs) which can exist in a spectral gap formed by poloidal mode coupling due to the toroidicity of the magnetic configuration are thought to be most dangerous AEs, because weak continuum damping is expected.[2] However, continuum damping of TAEs depends sensitively on the detailed structure of the magnetic configuration and density profile. Moreover, TAEs may be damped further by radiative damping,[3] which also sensitively depends on the magnetic configuration and the plasma parameters, i.e., temperature, ion mass, and so on. Prediction of the stability of the TAEs in a burning plasma is very difficult because complex kinetic approaches in a realistic magnetic configuration are necessary to evaluate these damping rates accurately. Therefore, experimental measurement of the damping rate of AEs is strongly required to evaluate the stability reliably and to provide data for comparison with theoretical models. In the Joint European Torus (JET) and Alcator C-Mod tokamaks,[4,5] measurements of damping rate were successfully carried out by an active diagnostic method where the damping rate is derived from a frequency response for externally applied oscillatory magnetic perturbations. It was found in JET that the measured damping rates for low-n (n is the toroidal mode number) TAEs increase with the increase in the magnetic shear, elongation and triangularity in a plasma.[6] On the other hand, this tendency was not observed for the damping rate of intermediate-n TAEs in Alcator C-Mod.[7] The reasons of this discrepancy are under investigation.

In helical systems, various types of AEs have been observed in W7-AS, the Compact Helical System (CHS), and the Large Helical Device.[8–13] Direct measurement of the damping rate of AEs is also required to understand the stability of AEs in these helical plasmas and predict the stability of future high temperature plasma against AEs. The first measurement of the damping rate of low-n TAE in a helical/stellarator device was successfully carried out by application of oscillatory external magnetic perturbations to a low temperature plasma of the CHS.[14] The experimental results showed that the continuum damping is fairly large. Later, measurement of the damping rate of low-n TAEs was attempted in high temperature plasmas heated by high power neutral beam injection (NBI) on CHS, by using the same system developed in the previous low temperature experiment.[15]

This paper describes the details of TAE excitation experiments by application of external magnetic field perturbations to NBI heated CHS plasmas. This paper is organized as follows. In Sec. II, we describe the experimental setup for measuring AE damping rates in CHS. Especially, it is focused on the excitation scheme including the expected excited mode pattern on the flux surface. In Sec. III A, we show typical discharge waveforms and the characteristics of a frequency response function so-called "transfer function" of a plasma to applied magnetic perturbations. In Sec. III B, we discuss the possibility of AE excitation near the plasma edge by energetic beam ions, based on the experimental database of energetic ion driven MHD modes in NBI heated CHS plasmas. In Sec. IV, experimental data are compared with the shear Alfvén spectra and eigenfunctions calculated

with a numerical code, AE3D, for analysis of AEs in a three dimensional (3D) plasma. In Sec. V, possible damping mechanisms of TAEs excited by this electrode technique are discussed. Results of this experimental campaign are summarized in Sec. VI.

II. EXPERIMENTAL SETUP

The CHS is a heliotron/torsatron type device which has the poloidal period number $l=2$, the toroidal period number $N=8$, the major radius $R\sim 1$ m, and the averaged minor radius $\langle a\rangle \sim 0.2$ m. Two tangential beam lines of NBI of which the typical acceleration energy is from ~36 keV to 40 keV are employed for coinjection heating by hydrogen beams as a main heating scheme. The total absorbed power of the NBI is about 1.7 MW in the present experiments. Electron density is controlled over a wide range by puffing of hydrogen.

Two electrodes have been installed in CHS separated by 180° away toroidally, as shown in Fig. 1(a), for the excitation of currents which are extracted along the magnetic field line by ac-biased electrodes. The electrode consisting of a 10 mm(=a)×30 mm(=b) stainless-steel plate is positioned perpendicularly to the line of force of confinement magnetic field and its position is adjusted near the plasma edge shot by shot, by using a mechanical adjustment, as shown in Fig. 1(b). An ac voltage is applied to each electrode with respect to the vacuum vessel wall by using a bipolar power supply and induces an ac current along the field line. In this experimental campaign, the center of the electrode plate was located at the normalized radius, $\rho=r/a\sim 0.85$, of which position was determined from the two conditions of minimum plasma disturbance and larger electrode current. The magnitude of the driven current is usually dominated by electron saturation current of the electrode in the case that the applied positive voltage is much larger than electron temperature and is proportional to the size of the electrode surface area normal to the line of force of the confining magnetic field. For the electrodes employed in the experiment, fairly large ion saturation currents are expected such as $I_{\mathrm{sat}}^{i}\sim 30$ A, where the electron temperature and electron density are assumed to be 40 eV and 2×10^{19} m^{-3}, respectively, as shown in Fig. 2(a). However, the electrode current will be limited to $I_{\mathrm{ant}}\sim 8$ A because of the capability of the power supply. Thus, the waveform of electrode current is almost sinusoidal without having an asymmetric shape. The current generates ac magnetic perturbations to excite stable AEs in a plasma. The frequency f_{ext} of applied magnetic perturbations is widely swept from several kHz to 300 kHz by a function generator controlled with a personal computer, in order to cover the range of expected TAE frequencies. The expected current path is depicted in Fig. 1(a). The length $L_{\parallel}$ of the current path extracted by a biased electrode is evaluated by a balance of particle (electron) fluxes which flow parallel and perpendicularly into a volume projected from the electrode along the field line,[16] that is,

$$\Gamma_{\parallel}A_{\parallel}+\Gamma_{\perp}A_{\perp}=0, \tag{1}$$

where $\Gamma_{\parallel}$ and $\Gamma_{\perp}$ are, respectively, expressed as

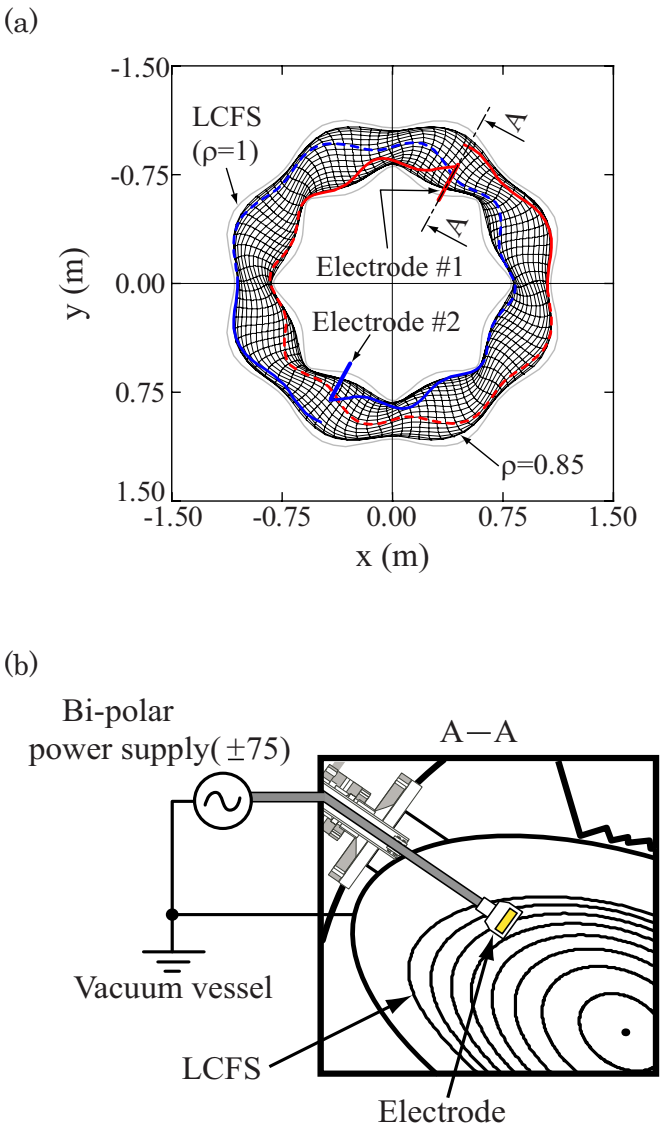

FIG. 1. (Color online) (a) Top view of the electrode arrangement and the shape of the magnetic surface at $\rho=0.85$. Red and blue curves on the surface are the expected current paths by ac biased electrodes in one toroidal excursion. (b) Cross-sectional view of an electrode system cut in section A-A where the electrode is installed.

$$\Gamma_{\parallel}=nV_{\parallel}/4 \tag{2}$$

and

$$\Gamma_{\perp}=nV_{\perp}=D_{\perp}\nabla_{\perp}n. \tag{3}$$

The $A_{\parallel}$ and $A_{\perp}$ are the normal cross-sectional area and whole side surface area of a flux tube projected along the magnetic field line from the electrode plate. If the conducting plate is shaped rectangularly, these surface areas are expressed as $A_{\parallel}=ab$ and $A_{\perp}=2(a+b)L_{\parallel}$, respectively. The sizes of the electrode are a in the radial direction and b in the poloidal direction. Here, $V_{\parallel}$ is the electron thermal velocity and $D_{\perp}$ is the perpendicular diffusion coefficient. If effective particle flux perpendicular to the field line is isotropic radially and poloidally, the length is finally derived from Eq. (1) with Eqs. (2) and (3) as

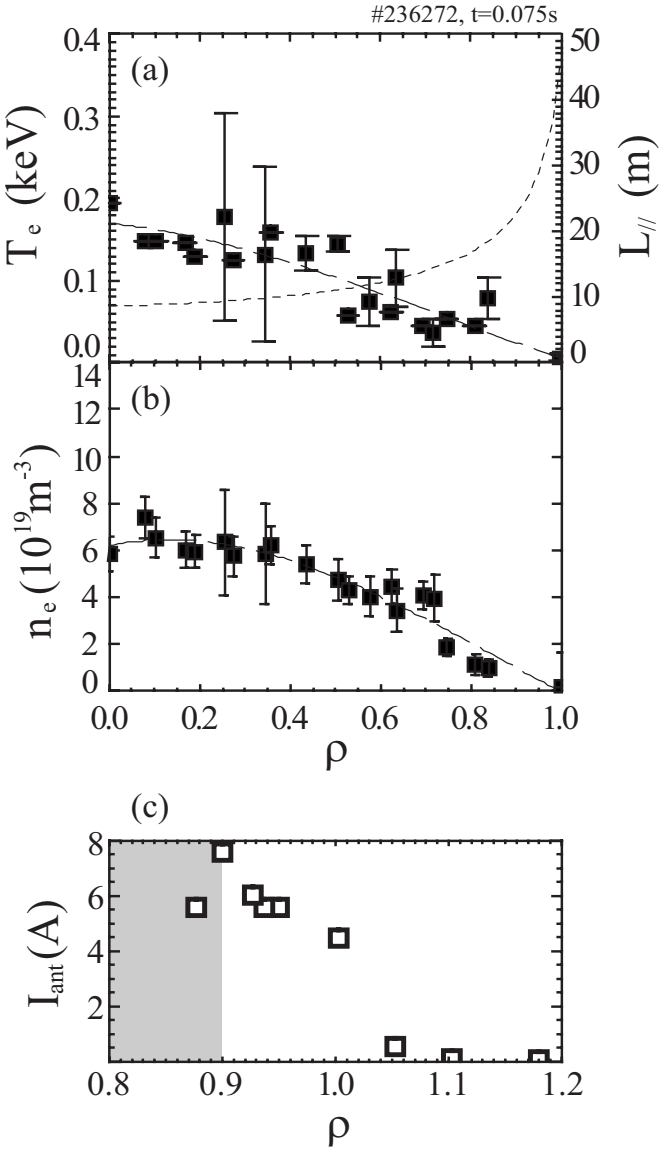

FIG. 2. Radial profiles of electron temperature (a) and (b) density obtained by Thomson scattering diagnostics. The calculated length of the current path is also shown by a dotted curve. (c) Radial dependence of the magnitude of electrode current, which is limited up to ~7 A due to the capability of the power supply.

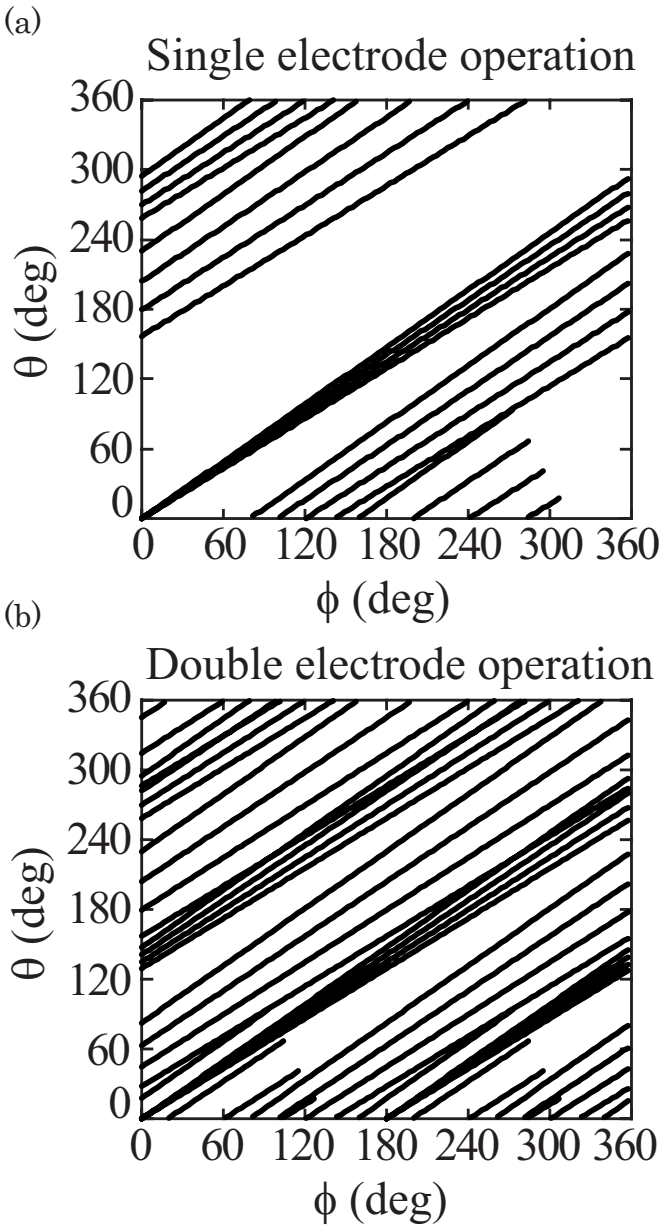

FIG. 3. Geometrical pattern of the currents induced by electrodes on the $\theta-\phi$ plane, where θ and ϕ are, respectively, poloidal and toroidal angles in the Boozer coordinates. The electrode is inserted at $\rho=0.85$. The rotational transform at the position that the conductive plate of electrode covered for $\rho=0.8-0.9$ is $\iota/2\pi=0.72-0.82$. (a) Pattern in single electrode operation and (b) that in double electrode operation.

$$L_{\parallel} = \frac{V_{\parallel}}{D_{\perp}} \frac{a^2 b}{8(a+b)}. \tag{4}$$

The thermal velocity of the electron is much faster than that of the ion, so that the driven current would be dominantly carried by electrons. The length of the current path $L_{\parallel}$ is determined by electron temperature, as shown in Fig. 2(a), where Bohm diffusion is assumed as $D_{\perp}$. In this experiment, a typical length of the current path $L_{\parallel}$ is estimated to be ~18 m when the electrode is placed at $\rho \sim 0.8-0.85$ where the electron temperature is ~40 eV [Fig. 2(a)].

The geometrical structure of the applied magnetic field perturbations is inferred by tracing the current path launched from the electrodes on the flux surface. In this experiment, two types of operation mode of electrodes were adopted, that is, "single electrode operation," where only one electrode is activated as a single Langmuir probe, and "double electrode operation," where two electrodes are activated as two single Langmuir probes with the same polarity. Figure 3 shows the current path on the Boozer coordinate $\theta-\phi$ plane for single and double electrode operations, where θ and ϕ are, respectively, the poloidal and toroidal angles. The Fourier spectrum of the excited magnetic field perturbation can be specified by an arrangement of current paths which is controlled by the number of electrodes and the phase relation among the electrodes. The Fourier spectrum of electrode current pattern is evaluated as

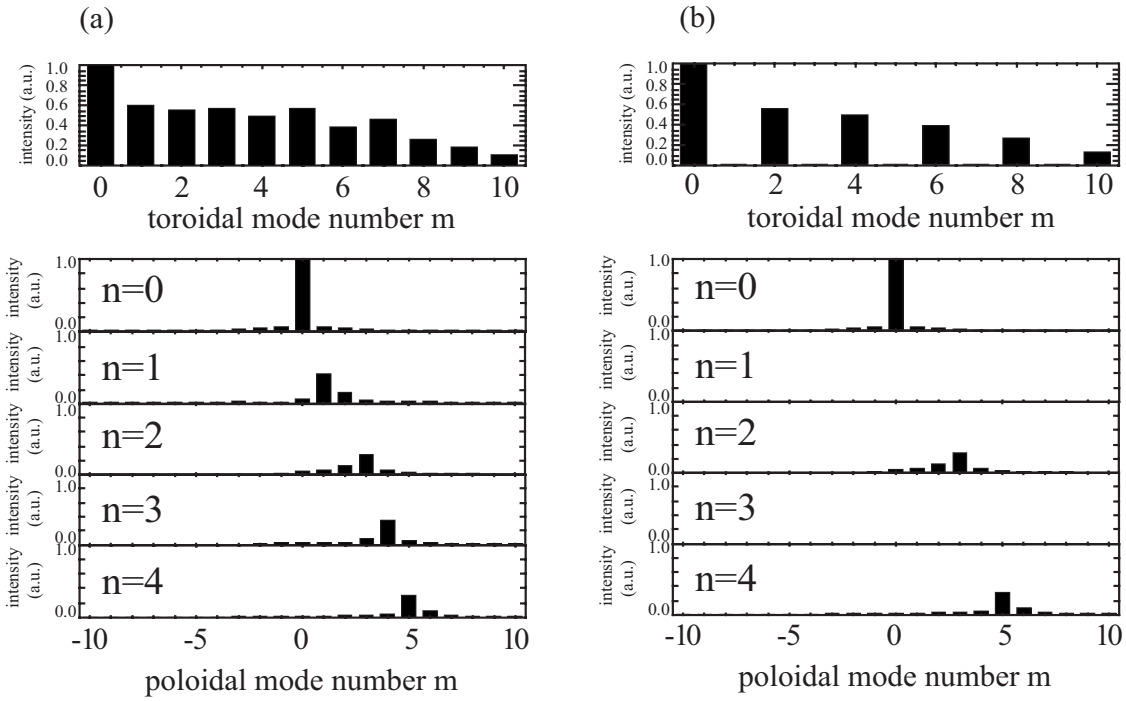

FIG. 4. Mode spectra of the current path pattern driven by biased electrodes in two cases of (a) single electrode operation and (b) double electrode operation, of which patterns are shown in Fig. 3.

$$I_{m,n} = \int \int J(\rho, \theta, \phi) e^{-i(m\theta - n\phi)} d\theta d\phi. \quad (5)$$

The calculated Fourier spectra of electrode currents in "single" and "double" electrode operations are shown in Figs. 4(a) and 4(b), respectively. In the single electrode operation, perturbations with many low toroidal mode numbers such as $n=0,1,2,3$ and so on can be excited having appreciable magnitude. On the other hand, the poloidal mode number is relatively concentrated around a certain m number which depends on n, as seen from Fig. 4(a). In the double electrode operation, perturbations with even toroidal modes such as $n=0,2,4$ and so on can be dominantly excited. The spectrum of m-number for each n has a similar character to that in single electrode operation. This character of the m-number distribution is related to the rotational transform at the position where the electrode is placed. In an actual experiment, the lowest toroidal mode number $n=1$ mode for the former operation and $n=2$ mode for the latter will be expected to be dominantly excited because it has the highest magnitude except the peculiar mode $n=0$. Although $n=0$ perturbation may have a potentiality to excite the $n=0$ global AE (GAE), the frequency range exceeds the sweeping range of the electrode current frequency in the present experiment and no response is expected. Magnetic perturbations generated by the above-mentioned current paths are also expected to be dominated by the $n=1$ and $n=2$ Fourier component for single and double electrode operations, respectively. TAEs of which gaps are nearest to the exciter electrodes are thought to be predominantly excited by magnetic perturbations that are generated by the electrodes at $\rho \sim 0.85$. Actually, TAEs whose gaps are in the region of $0.7 < \rho < 1.0$ were excited by this technique because the applied fields would be decayed away from the electrode position. In CHS plasmas of this experimental campaign, the gaps of $n=1$ and $n=2$ TAEs which are in the above-mentioned region of $0.7 < \rho < 1$ are located to be $\rho \sim 0.8$ for $n=1$ TAE, and $\rho \sim 0.7$ and ~ 0.9 for $n=2$ TAE. Actually, these TAEs were successfully excited.

III. EXPERIMENTAL RESULTS

Discharge waveforms of a typical NBI-heated hydrogen plasma are shown in Fig. 5, where the toroidal magnetic field is $B_t=0.9$ T, and the magnetic axis position of the vacuum field is $R_{ax}=0.921$ m. The line-averaged electron density was increased by gas puffing up to $\sim 4.5 \times 10^{19}$ m^{-3} to minimize the energetic ion drive for AEs. The volume-averaged total beta value, including the energetic ion component, is about 0.5%. In this shot, the rotational transform profile is dominantly determined by the finite beta effect, because the net plasma current is fairly small (≤ 3 kA). In a typical single electrode operation shown in Fig. 5(e), the frequency f_{ext} of the applied magnetic perturbations was swept linearly in time from 10 to 200 kHz for 0.1 s to search for expected TAE frequencies. In a typical double electrode operation, the frequency f_{ext} was swept from 10 to 300 kHz. The sweeping range of f_{ext} was determined to include the range of TAE gap frequencies in the present experimental conditions. In this shot shown in Fig. 5, the TAEs and GAE destabilized by energetic ions are clearly observed during the NBI phase. The intensity of magnetic fluctuations along the swept frequency of the externally applied perturbations is shown in Fig. 5(e). The enhanced fluctuation intensity in the range of $f < 130$ kHz is mainly responsible for the above-mentioned TAEs and GAE destabilized by energetic ions. The response from stable AEs to applied perturbations should be searched

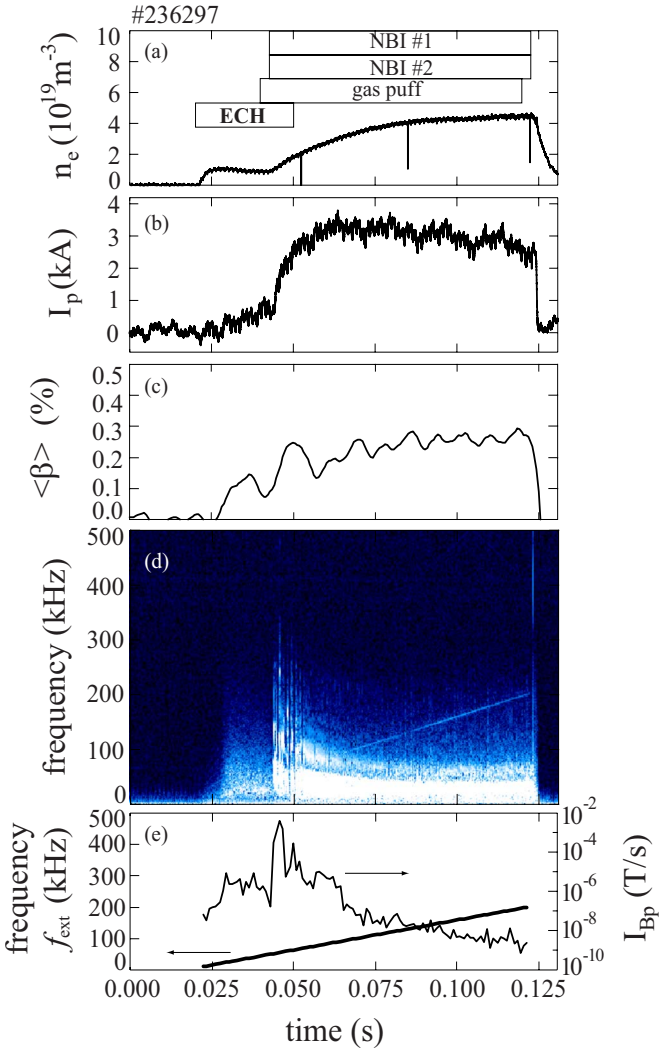

FIG. 5. (Color online) Waveforms of a typical discharge where electrode operations were performed: (a) line-averaged electron density, (b) toroidal current, (c) volume-averaged bulk plasma beta, (d) spectrogram of magnetic probe signal, and (e) sweep function of applied perturbation and magnetic fluctuation along the sweep function.

for in the latter phase of $t>0.085$ s where the frequency of these energetic ion driven modes goes down to less than ~100 kHz.

A. Observation of resonant responses to applied perturbations

A plasma having some spectral gaps such as TAE gaps in the shear Alfvén spectrum will respond to alternating magnetic perturbations as a vibrating viscous damping system with multiple degrees of freedom. The frequency response function, that is, the transfer function of the plasma, $G(\omega)$, will be expressed as

$$G(\omega)_{\text{model}} = \frac{B(\omega)}{A(\omega)} = \sum_{r=1}^{N} \left\{ \frac{R_r}{i(\omega-\Omega_r)+\gamma_r} + \frac{R_r^*}{i(\omega+\Omega_r)+\gamma_r} \right\}. \quad (6)$$

Here, ω, Ω_r, γ_r, R_r, and R_r^* are, respectively, the driving angular frequency, angular eigenfrequency that characterizes the resonance, damping rate, and the residue and its conjugate term at the rth resonance. The quantity $B(\omega)$ stands for the Fourier transform of magnetic fluctuations detected by a magnetic probe. As the input signal $A(\omega)$, the electrode current can be adopted instead of externally applied magnetic field perturbations. All signals of electrodes and magnetic probe arrays are acquired as digitized data and analyzed by appropriate data processing software, after every plasma shot where the AE excitation experiments were performed.[14] The transfer function was derived from Fourier transform of input and output signals evaluated as a function of the driving frequency of the electrode current.

A resonant response can be identified from the following characters of the transfer function: the appearance of a clear peak in the absolute value of $G(\omega)$ and a sudden change in the sign of the phase of $G(\omega)$, that is, $\tan^{-1}\{\text{Im}[G(\omega)]/\Re e[G(\omega)]\}$. Thus derived transfer functions $G(\omega)=B(\omega)/A(\omega)$ for the applied magnetic perturbations are shown with solid curves in Figs. 6(a)–6(c), for the single and double electrode operations. It should be noted that a peak less than $f\sim 130$ kHz in the absolute value of the transfer function $|G(\omega)|$ shown in Fig. 6 or Fig. 7 is caused by AEs destabilized by energetic ions. The part $f<130$ kHz should be removed as background noise to extract a resonant peak related to AEs purely excited by the electrode current. In single electrode operation (Fig. 6), a clear resonant peak is identified in the frequency range of 130–190 kHz. In double electrode operation (Fig. 7), two resonant peaks are identified in the range of 130–300 kHz. It should be noted that the transfer functions shown in Figs. 6 and 7 are still deformed by the noise component, even if the energetic ion driven part less than 130 kHz is removed. The noise components in $\text{Re}[G(\omega)]$ and $\text{Im}[G(\omega)]$ are well expressed by a linear function of ω as $K\omega+L$, where K and L are complex constants. These constants K and L are evaluated so that $\text{Re}[G(\omega)]$ and $\text{Im}[G(\omega)]$ should have an even or odd function around an expected resonant frequency to express the clear resonance character. The transfer functions where the noise components were subtracted are shown in Figs. 6(d)–6(f) and Figs. 7(d)–7(f), A resonance frequency Ω_r, its damping rate γ_r, and R_r and R_r^* can be derived from the transfer function by curve fitting to Eq. (3). If the resonance frequency Ω_r agrees well with the resonance frequency used in the above-mentioned subtraction procedure of the noise, we can get final results having the best fit with the model function Eq. (3).

It should be noted that any resonance characters in the range less than 300 kHz should be eliminated in the external excitation circuit in order to measure the damping rate of excited AEs accurately. In order to investigate whether or not the external circuit has any resonances which are not related to AEs, magnetic perturbations of up to 300 kHz were applied to a low density electron cyclotron heating (ECH) plasma where the lowest TAE gap frequency in the plasma edge region is well above 300 kHz. The transfer function of that case does not exhibit any resonance characters. It is concluded that the effects of external circuit on measurement of damping rate of AEs can be neglected.

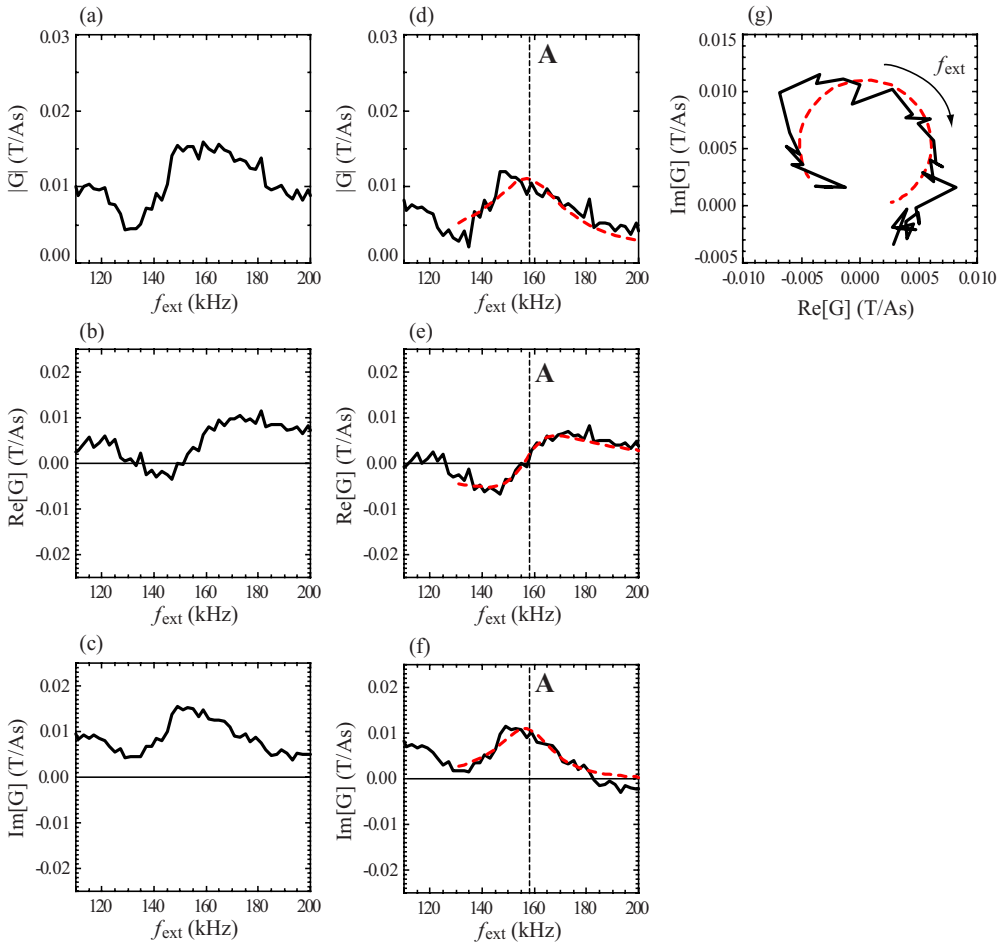

FIG. 6. (Color online) Transfer function obtained in single electrode operation: (a) absolute value, (b) real part, and (c) imaginary part. (d)–(f) show the transfer function in which the noise component is removed from the raw data for (a)–(c) in order to extract the resonant response. (g) Nyquist plot for the extracted transfer function. Long-dashed curve indicates a best fitted transfer function. Vertical dotted line indicates the eigenfrequency of the excited resonant mode.

In the single electrode operation, the resonant frequency and the damping rate were obtained by the above technique as $f_o=157$ kHz and $\gamma/\omega_o \sim 9\%$, where $\omega_o=2\pi f_o$ is the eigenangularfrequency. Moreover, the locus of the complex vector $G(\omega)$ draws a circle when the frequency f_{ext} is swept from 140 to 190 kHz. On the other hand, two resonant peaks are identified in double electrode operation. One is a resonance peak at $f_o=172$ kHz and its damping rate $\gamma/\omega_o \approx 12\%$. Another is at $f_o=276$ kHz and the damping rate $\gamma/\omega_o \approx 12\%$.

The mode numbers m and n for the above-mentioned resonant responses were determined by using magnetic probe arrays. Figure 8 shows the phase lag of each magnetic probe in a toroidal array for the above-mentioned resonant responses. If AEs are excited by applied magnetic perturbations, they can propagate in both toroidal directions. The mode excited by the single electrode operation is $n=-1$ and propagates in the counter clockwise (CCW) direction, where CW and CCW propagation is respectively indicated with positive and negative n. Both low frequency and high frequency modes excited by the double electrode operation propagate in the CW direction having $n=2$, as seen from Fig. 8. Basically, externally excited TAEs can propagate along the lines of force of equilibrium magnetic field in both directions. In a toroidally symmetric configuration such as tokamak, stable AEs excited by magnetic perturbations will propagate in parallel and antiparallel directions. In a 3D configuration such as helical/stellarator configuration, magnetic configuration is not necessarily symmetric in the toroidal direction. It is thought in this situation that thus excited stable AEs can propagate predominantly to a certain direction, although the reason why the propagation direction is determined to be approximately one directional is not clarified yet. On the other hand, AEs destabilized by energetic ions propagate in a certain direction depending on injection direction of NBI and the direction of ion diamagnetic drift.

In the magnetic configuration of low beta CHS plasma, the rotational transform increases toward the plasma edge. Accordingly, the TAE gap frequency increases toward the plasma edge. Even if large magnetic perturbations are applied to the plasma externally, magnetic perturbations necessary for excitation of TAEs in the plasma interior region may be reduced considerably due to continuum damping near the plasma edge. Moreover, TAEs in the plasma interior region are strongly destabilized by energetic ions. Then it becomes difficult to derive the accurate damping rate by removing the

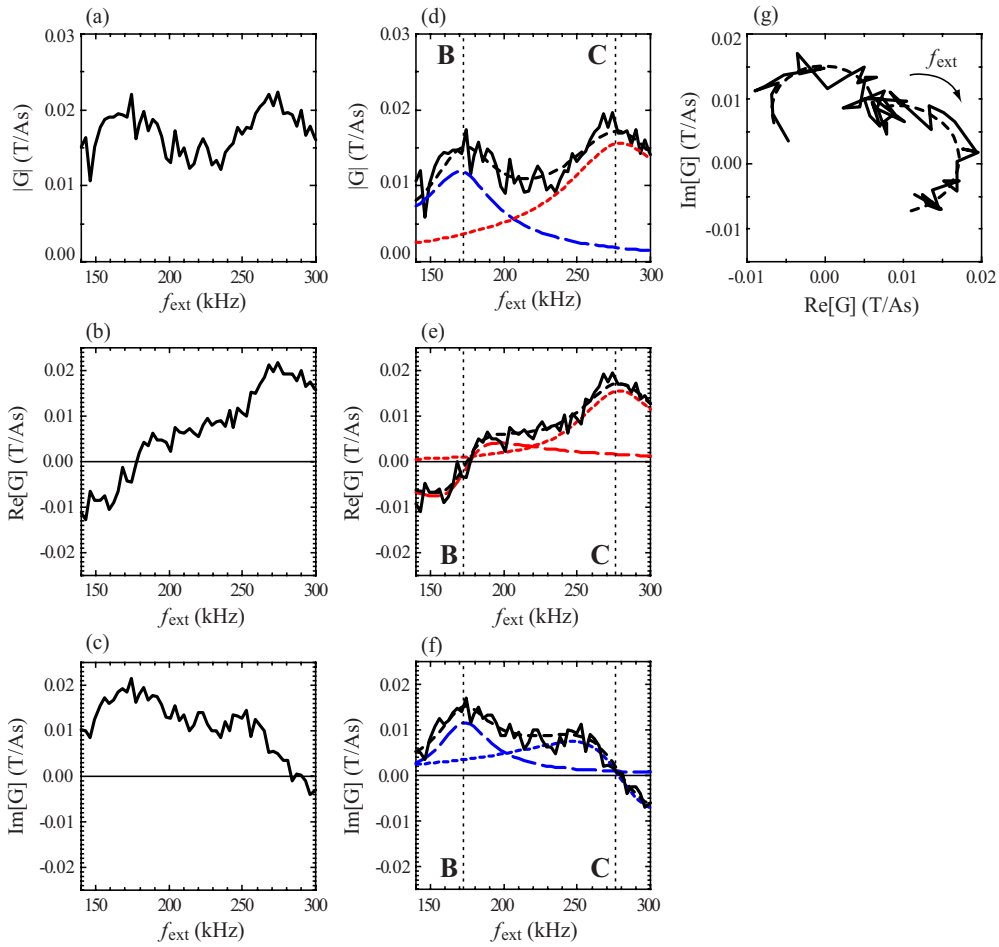

FIG. 7. (Color online) Transfer function obtained in double electrode operation: (a) absolute value, (b) real part, and (c) imaginary part. (d)–(f) show the transfer function in which the noise component is removed from the raw data for (a)–(c) in order to extract resonant response. (g) Nyquist plot for the extracted transfer function. Long-dashed curve indicates a best fitted transfer function of the lower frequency resonant mode (~172 kHz). Dotted curve indicates that of the higher frequency mode. Vertical dotted lines indicate these resonant modes. (g) Nyquist plot for the extracted transfer function.

effect of energetic ion drive. This may be a reason why only TAEs having the gaps in the plasma edge were excited by application of external magnetic perturbations.

In this experimental campaign, the toroidal magnetic field strength B_t was selected to be 0.9 and 1.4 T in order to a target plasma with 54 GHz ECH. The line averaged electron density also changed with the change in B_t. Therefore, we compare the resonance frequencies observed in various CHS plasmas with the predicted TAE gap frequencies. This result is shown in Fig. 9. The observed resonance frequencies agree with the TAE frequencies having small deviations. These deviations are thought to be caused by error in electron density at the gap location and finite width of the gap.

B. Effects of energetic ion drive on externally excited resonant modes

As mentioned in the previous subsection, the damping rate was successfully derived through the analysis of the transfer function in NBI heated plasmas. The TAEs excited by applied magnetic perturbations have the gap near the plasma edge where energetic ion drive is inferred to be small. In order to confirm this prediction, the density range where TAEs are destabilized by energetic ions was investigated in the magnetic configuration where the electrode experiments were carried out. In the low density phase ($\langle n_e \rangle \leq 2 \times 10^{19}$ m^{-3}), several energetic ion driven AEs are identified in the frequency range up to ~250 kHz. In the high density phase $\langle n_e \rangle \geq 3 \times 10^{19}$ m^{-3} where the excitation experiments of stable AEs by the inserted electrodes were carried out, only $m=3/n=1$ and $m \sim 5/n=2$ modes persist in the lower frequency range of $f<100$ kHz.[17] The observed mode frequency for $m=3/n=1$ modes is thought to be GAE near the plasma central region where TAE gap is not generated due to the increase in the rotational transform. The other remaining mode $m \sim 5/n=2$ is consistent with TAE of which gap is formed through $m=5$ and $m=6$ mode coupling and is located at $\rho \sim 0.35$ in the present experimental condition. It should be noted that the gap locations of $n=1$ and $n=2$ TAEs are predicted to be almost independent of the averaged total plasma beta value up to 0.8%, which will be achieved in the electron density scan of this experiment campaign with ~1.7 MW NBI power. That is, the location of $n=1$ TAE gap by $m=1$ and $m=2$ coupling is $\rho \sim 0.8$ and that by $m=2$ and $m=3$ coupling is $\rho \sim 0.45$. Those of $n=2$ TAE gaps by $m=2$ and 3, $m=3$ and 4, $m=4$ and 5, and $m=5$ and 6 couplings are, respectively, $\rho \sim 0.9$, $\rho \sim 0.7$, $\rho \sim 0.55$, and

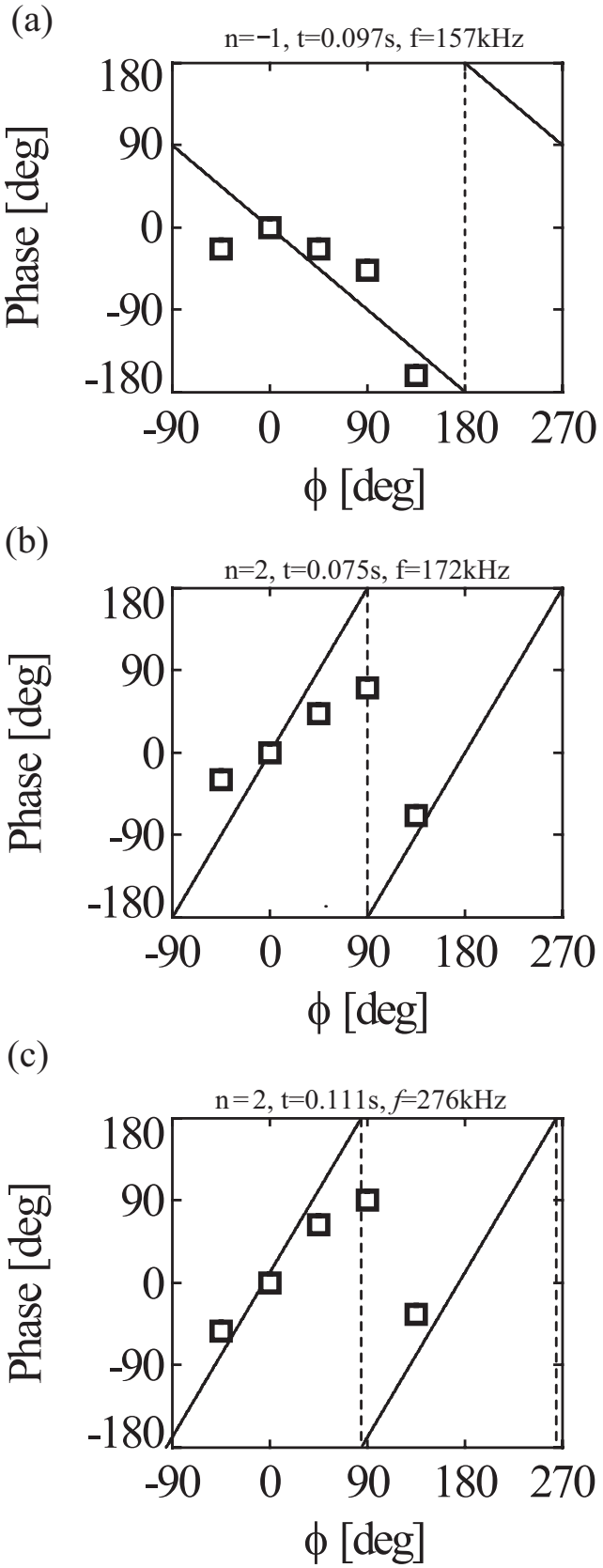

FIG. 8. Toroidal phase dependences in the magnetic probe array for the observed resonant modes in single electrode operation (a) labeled A in Fig. 6 and double electrode operation.(b) labeled B and C in Fig. 7. The mode A propagates in the CCW direction of the torus and has $n=1$. The modes B and C propagate in the CW direction and have $n=2$.

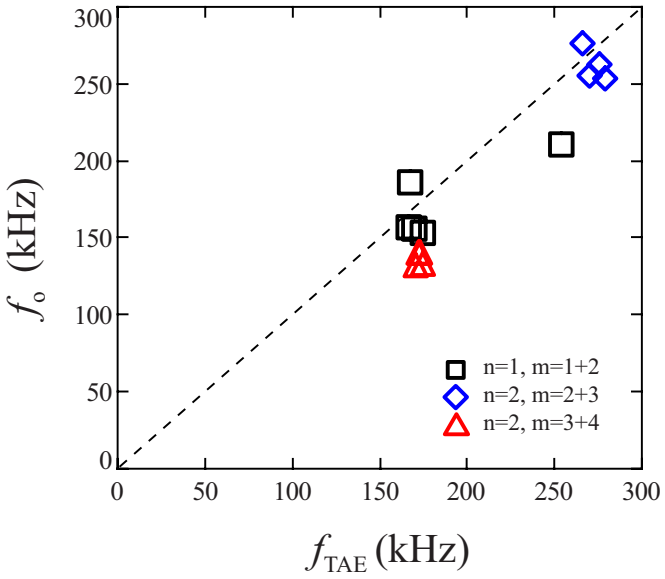

FIG. 9. (Color online) Comparison between TAE gap frequencies f_{TAE} derived from line averaged electron density and measured eigenfrequencies f_o. The broken line traced $f_{TAE}=f_o$ condition.

$\rho\sim0.35$. Accordingly, energetic-ion driven TAEs of which gaps are located near the plasma edge, $\rho>0.6$, are suppressed in the high density range, because energetic ion drive will be very small there. It is concluded that TAEs in the plasma peripheral region of $\rho>0.6$ excited by electrodes are not affected by energetic ions.

IV. COMPARISON WITH COMPUTATIONAL RESULTS OF ALFVÉN EIGENMODES

The stability of AEs depends on the radial profile of the energetic ion pressure and the radial structure of the shear Alfvén spectrum, which is determined by the radial profiles of bulk ion density and the rotational transform. First, we compare the observed coherent modes excited by the application of external magnetic perturbations and energetic ions with the calculated shear Alfvén spectra and attempt to identify them. The shear Alfvén spectra were calculated, using the MHD equilibrium calculated by the VMEC code with the experimentally observed net plasma current. In the electrode experiments, the net plasma current is fairly low ($\lesssim3$ kA) because of a fairly high electron density, as seen from Fig. 5. This current will consist of appreciable bootstrap current and less NBI driven current. Here, a plausible current density profile was assumed to be a broad profile, that is, $j_\phi/j_0=(1-\rho^2)^{0.5}$. Moreover, the following assumptions were introduced that the dominant impurity is fully ionized carbon and the effective charge profile is $Z_{eff}=3$ in whole plasma region.

In the single electrode operation, the observed frequency of the resonant response having an $n=1$ mode structure ($f_o=157$ kHz) is clearly distant from the frequency range of these fast ion driven modes, as seen from the shear Alfvén spectra in Fig. 10(a). The frequency of the externally excited resonant mode is located just inside the TAE gap generated

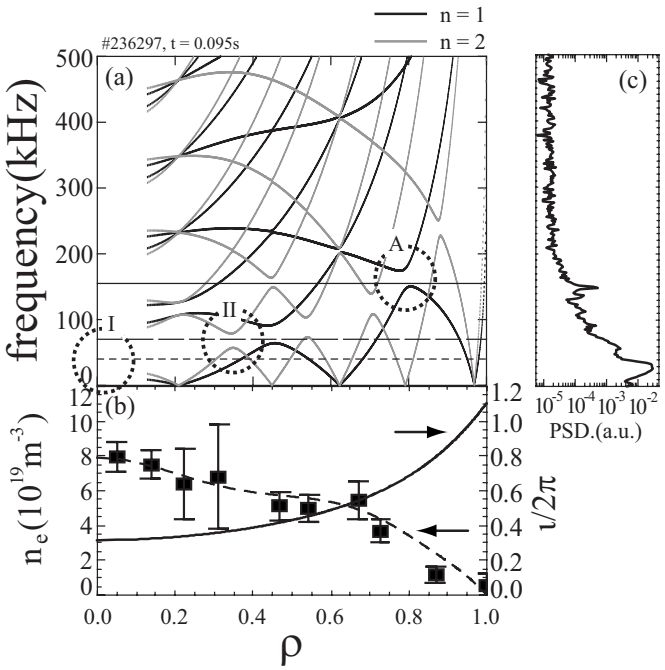

FIG. 10. (a) Calculated shear Alfvén spectra of $n=1$ (thick curve) and $n=2$ (thin curve) modes for the plasma at $t=0.095$ s in the discharge (No. 236297) as shown in Fig. 6, where single electrode operation was performed. Horizontal dotted line and dashed line indicate the most coherent fluctuation $n=1$ and $n=2$ modes driven by energetic ions. Black broken circle labeled A indicates the TAE gap location corresponding to the $n=1$ observed resonant response to applied magnetic perturbations. The circles labeled I and II indicate the gap locations of $(m,n)=(5,2)$ TAE and $(m,n)=(3,1)$ GAE driven by energetic ions. (b) Radial profile of electron density and the rotational transform. (c) Power spectral density of magnetic probe signal obtained at $t=0.095$ s.

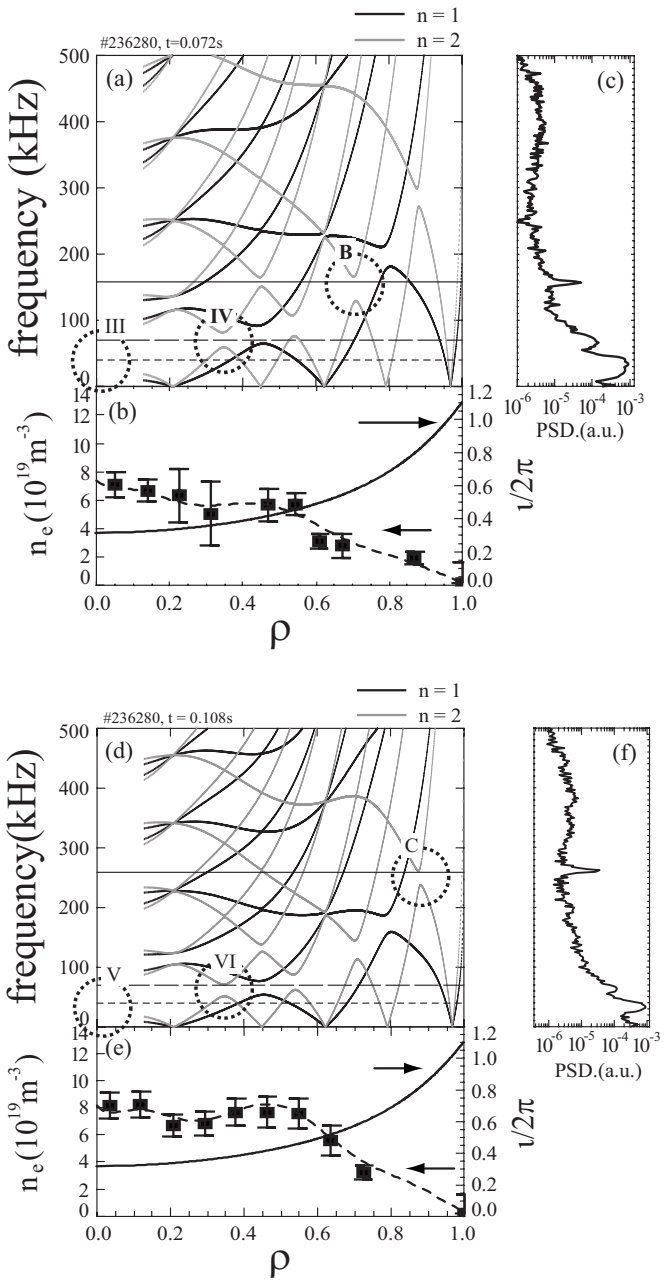

FIG. 11. Calculated shear Alfvén spectra of $n=1$ (thick curve) and $n=2$ (thin curve) modes for the plasma (No. 236280), where double electrode operation was performed. The shear Alfvén spectra (a) and (d) are calculated for two time slices of $t=0.072$ s and $t=0.108$ s when two resonant modes were excited by electrodes. The circles labeled B and C indicate the TAE gaps corresponding to the observed $n=2$ resonant modes. The circles labeled IV and VI indicate the $(m,n)=(5,2)$ TAE gaps corresponding to the observed mode driven by energetic ions. The circles labeled III and V indicate the mode location of $(m,n)=(3,1)$ GAE. (b) and (e) are electron density profiles and (c) and (f) the power spectra of magnetic fluctuations.

by poloidal mode coupling of the $m=1$ and $m=2$ Fourier components. Accordingly, it is thought to be an $n=1$ TAE related to the gap.

In the double electrode operation, two resonant modes with $|n|=2$ are identified in the transfer function, as shown in Fig. 7. In this section, we first compare the experimental data with the $n=2$ shear Alfvén spectra. These two frequencies, respectively, indicated by solid horizontal line in Figs. 11(a) and 11(d) agree well with the relevant TAE gaps in the calculated shear Alfvén spectrum. The TAE gap with higher frequency is formed by $m=2$ and $m=3$ coupling. The other gap with lower frequency is formed by $m=3$ and $m=4$ mode coupling and is located more inside that of the low frequency mode. Both TAE gaps are in the plasma peripheral region of $\rho>0.7$. As discussed in Sec. III B, energetic ion drive is thought to be very small in these TAE gaps near the plasma edge.

In the high density plasmas in which both electrode operations were carried out, two characteristic types of energetic ion driven modes having $m=3/n=1$ and $m\sim5/n=2$ were still observed in the lower frequency range less than ~100 kHz, as mentioned in Sec. III B. The energetic ion driven $m=3/n=1$ modes are thought to be global Alfvén eigenmodes (GAEs) of which frequency is located just above the $m=3$ shear Alfvén continuum and is not in a TAE gap.[18,19] The observed frequency of $m=3/n=1$ seems to be located just above the maximum of the $m=3/n=1$ spectrum. The gap location of the $m\sim5/n=2$ TAE, which is still observed in the higher density regime, is in the plasma core region of $\rho\sim0.35$, as seen from the shear Alfvén spectra in Figs. 10 and 11. This TAE, of which gap resides in the plasma core region can be destabilized by appreciable amount of energetic beam ions even in this high density plasma. On the other hand, as mentioned in Sec. III B, it is

concluded that energetic ion drive is very weak in the plasma edge region of $\rho \geq 0.6$.

In the plasma edge region with high magnetic shear, continuum damping is inferred to be considerably large.[20] A possibility of continuum damping may be seen from the shape of the calculated eigenfunction of TAEs excited by electrodes. The eigenfunction of observed TAEs driven by energetic ions and applied magnetic perturbations were calculated by using the AE3D code, which was developed to calculate AEs in a low beta incompressible stellarator plasma.[21] All derived eigenfunctions have sharp spikes and/or sharp changes caused by numerical divergence related to the Alfvén resonance, as shown in Fig. 12. The eigenfunction of the $n=1$ mode ($f_o=155$ kHz) excited by single electrode operation does not have a sharp spike of the $m=1$ Fourier component very near the last closed flux surface [Fig. 12(a)]. This sharp spike is thought to be caused by an interaction with the $m=1$ continuum which increases very rapidly due to a considerable decrease in electron density and increase in the rotational transform there. This interaction may lead to a large damping rate as it was measured experimentally by the electrode method, as shown in Sec. III A. On the other hand, the eigenfunction of the externally excited $|n|=2$ lower frequency mode ($f_o=158$ kHz) has a sharp spike caused by an interaction with the $m=3$ continuum at $\rho \sim 0.85$, where numerical divergence occurs due to the Alfvén resonance there [Fig. 12(b)]. It also has a spike at $\rho \sim 0.45$ due to interaction with the $m=4$ continuum. The eigenfunction of the higher frequency mode ($f_o=259$ kHz) excited by electrodes also indicates a similar character caused by interactions with $m=3$ and $m=2$ continua [Fig. 12(c)]. These interactions with shear Alfvén continua will lead to a large damping rate, as shown in Sec. III A.

In addition, the eigenfunction of the observed energetic ion driven $m \sim 5/n=2$ TAE is also shown in Fig. 12(d) for comparison with those of externally excited TAEs. It is concluded that the $m \sim 5/n=2$ TAE was destabilized by intense energetic ion drive in the plasma core region despite of appreciable continuum damping at $\rho \sim 0.5$. The eigenfunction of the $m=3/n=1$ mode, however, cannot be calculated because the calculation has difficulty near the magnetic axis due to a failure of the MHD equilibrium reconstruction by the VMEC code.

V. DISCUSSION

In this excitation experiment of AEs by electrodes inserted in the plasma edge, stable TAEs of which spectral gaps reside in the plasma edge region were excited and their damping rates were obtained experimentally. The damping rates are considerably large, that is, ~9%–12% of the eigenfrequencies. So far, no numerical code is available to evaluate the damping rate of TAEs in LHD plasmas. Here, we compare the experimentally obtained damping rate of TAEs with theoretical values of the damping rate using analytic formulae for TAEs in a tokamak plasma. Continuum damping,[22,23] electron Landau damping,[24] radiative damping,[3] and collisional damping[25] are main candidates for the damping mechanisms of TAEs.

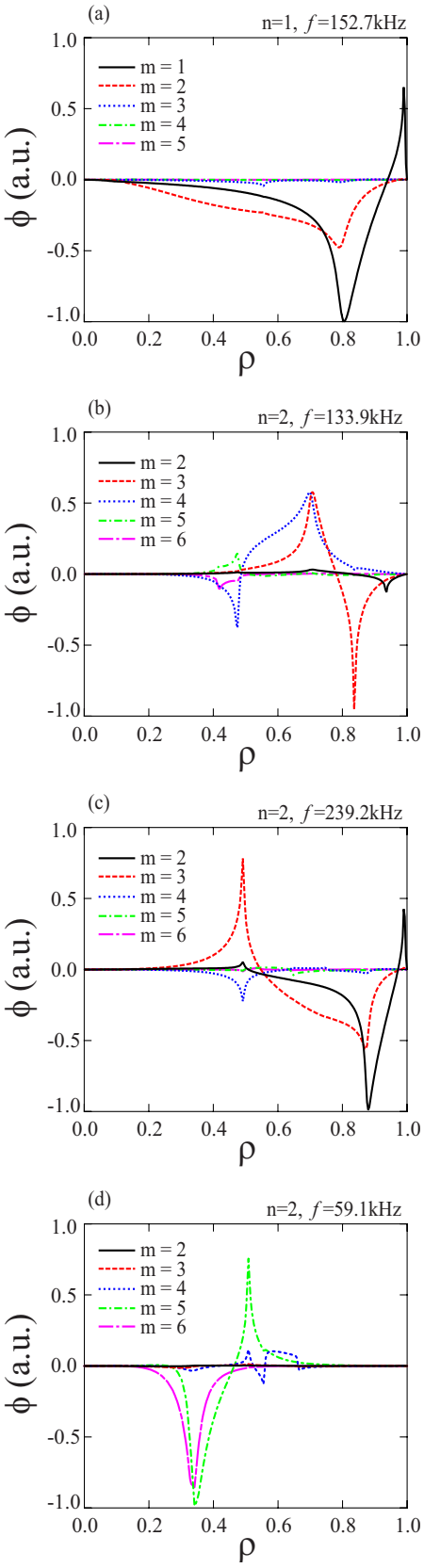

FIG. 12. (Color online) Eigenfunctions calculated by the AE3D code. Each eigenfrequency obtained by the code is indicated at the top and right-hand corner of each figure. (a) Calculated eigenfunction for the $n=1$ externally excited mode labeled A in Fig. 10. (b) Eigenfunction for $n=2$ externally excited mode labeled B in Fig. 11. (c) Eigenfunction for $n=2$ externally excited mode labeled C in Fig. 11. (d) Eigenfunction for energetic ion driven $(m,n)=(5,2)$ TAE of which gap is formed through coupling $m=5$ and $m=6$ Fourier modes.

The electron Landau damping rate, γ_e/ω_o, depends on the bulk electron beta β_e and the resonance condition between the thermal electrons and the shear Alfvén wave. The equation in which the $v_A/3$ sideband resonance is taken into account is expressed as[26]

$$\frac{\gamma_e}{\omega_o} = q^2\beta_e\left[g_m(x) + g_m\left(\frac{x}{3}\right)\right]. \tag{7}$$

Here, q is the safety factor. The resonance condition is expressed as the distribution function $g_m=(\pi^{1/2}/2)x(1+2x^2+2x^4)e^{-x^2}$ with $x=v_A/v_e$, where v_e is electron thermal velocity. The electron temperature in the gap region is in the range of $T_e\sim 0.1-0.3$ keV, so that the electron Landau damping rate is estimated to be $\gamma_e/\omega_o\sim 1\%$ or less in the edge region ($\rho>0.6$), as shown with a red broken curve in Fig. 13.

Electron collisional damping may be enhanced in the plasma edge region of low electron temperature. In Ref. 25, the following analytic form of Eq. (2) is presented:

$$\frac{\gamma_{ec}}{\omega_o} = -2.1\beta_e\left(\frac{v_e}{\omega_{\mathrm{TAE}}}\right)^{1/2}\left[\ln 8\left(\frac{2\omega_{\mathrm{TAE}}r}{Rv_e}\right)^{1/2}\right], \tag{8}$$

where ν_e, r, and ω_{TAE} are the electron collision frequency, radial position of TAE gap, and angular eigenfrequency of the TAE, respectively. Electron collisional damping $\gamma_{\mathrm{ec}}/\omega_o$ has the similar radial dependence with electron Landau damping but it is of the order of 0.1%, which is less than the above-mentioned collisionless electron Landau damping.

Even if an excited TAE frequency is inside the spectral gap, radiative damping is possible. We evaluate a simple analytic form of Eq. (42) in Ref. 3,

$$\frac{\gamma_k}{\omega_o} = -3\left[\frac{m(m+1)}{2m+1}\left(\frac{s}{2^{1/2}}\right)\frac{\rho_s}{r}\right]^{2/3}. \tag{9}$$

This damping depends on the magnetic shear s and the ion gyroradius ρ_s evaluated with electron temperature. This is $\gamma_k/\omega_o\sim 10\%$ for the above-mentioned TAEs excited by electrodes.

As seen from Fig. 12, calculated eigenfunctions of TAEs excited by electrodes indicate clear signatures of interaction with shear Alfvén continua, which lead to continuum damping. We adopted an analytic formula, Eq. (57) in Ref. 23, for calculation of the damping rate,

$$\frac{\gamma_c}{\omega_o} = \frac{\varepsilon}{2}\left[\frac{1}{g_0(s)} + \frac{1}{g_\infty(s)}\right], \tag{10}$$

where ε is inverse aspect ratio. The function g_0 is the damping rate for the parameter $m\hat{\varepsilon}\ll 1$ such that the adjacent TAE gaps are not well aligned to each other, where $\hat{\varepsilon}\equiv\varepsilon[\partial\ln(q^2/v_A^2)/\partial\ln q^2]^{-1}$. The function g_∞ is the damping rate in the $m\hat{\varepsilon}\gg 1$ limit that the TAE gaps are radially aligned well. These functions g_0 and g_∞ are given in Table I of Ref. 23. It should be noted that the formula is derived for high n TAEs in a tokamak plasma and may not be straightforwardly applied to the low n TAEs observed in CHS. However, this evaluation will give us important information about the magnetic shear effect on the damping rate. Continuum damping

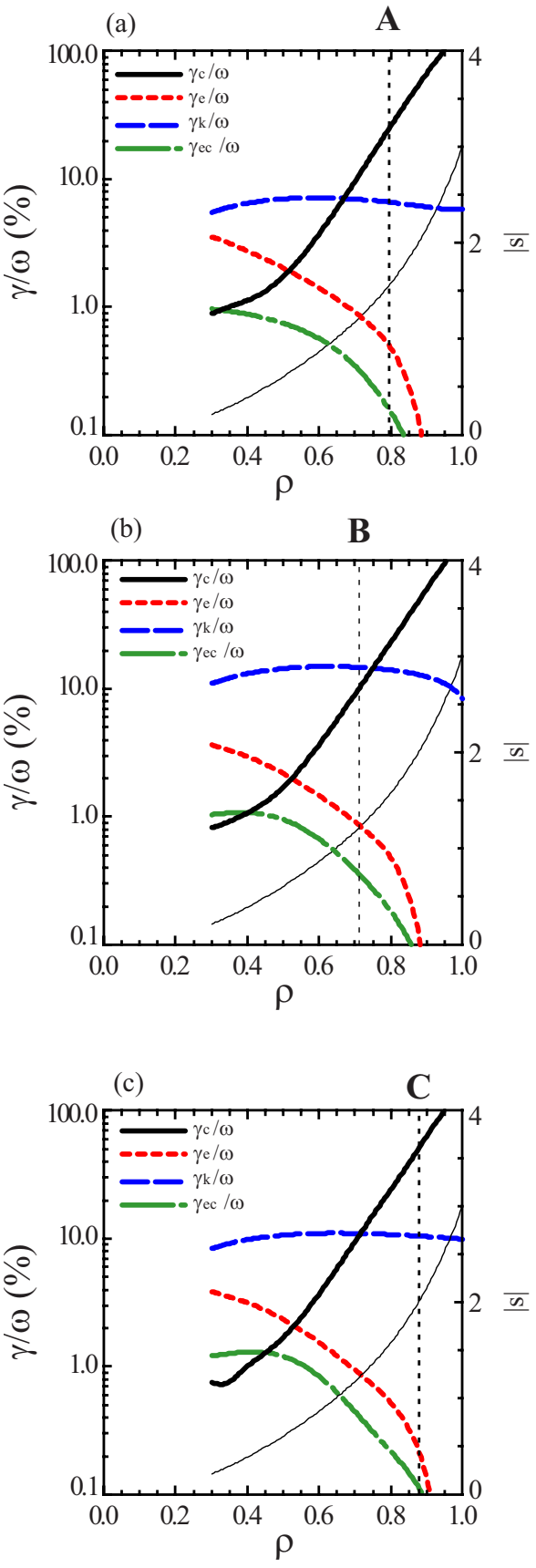

FIG. 13. (Color online) Calculated radial profiles of continuum damping rate (solid curve), radiative damping rate (blue dashed curve), electron Landau damping rate (red dotted curve), and collisional damping rate (green dashed-dotted curve) for TAEs labeled A, B, and C, respectively. Radial profile of global magnetic shear is also shown by thin solid curve. Vertical dotted line indicates the expected gap location.

mainly depends on the magnetic shear profile, so that the continuum damping near the edge is significant in the CHS plasma. Thus calculated results are shown with a solid curve in Fig. 13. The absolute value of the global magnetic shear was used in the calculation, because the damping rate is thought to be independent of the sign of the global magnetic shear. As seen from Fig. 13, continuum damping for these TAEs excited by electrodes is much larger than other damping mechanisms near the edge region. On the other hand, for the TAE gap at $\rho \sim 0.7$, continuum damping is still large, but the contribution of radiative damping becomes comparable to it. That is, the dominant damping rate is thought to be mainly due to continuum damping. The sum of the damping rates estimated for the above-mentioned mechanisms is by a factor of 2 or 3 larger than the measured damping rate, This may be caused by the fact that the analytic equation[23] is derived based on the assumption of high n TAE and it may not be directly applied to the present data of low n TAEs. More detailed analysis of continuum damping is necessary for a quantitative comparison between experimental data and theoretical ones.

VI. SUMMARY

The stability of TAEs in NBI-heated high density plasmas was investigated by the application of alternating magnetic field perturbations in CHS. The perturbations were generated by two electrodes inserted into the plasma edge being separated in the toroidal direction by 180°, of which method is favorable for the excitation of shear Alfvén waves. The transfer function that expresses the plasma response to applied perturbations was derived as a function of the drive frequency of the perturbations. A clear resonance peak in the transfer function obtained in single electrode operation was identified in the frequency range ($130 < f < 210$ kHz) well above AEs driven by energetic ions. Two resonance peaks in double electrode operation were identified. These observed resonance frequencies match very well with the TAE gaps calculated by the AE3D code. The TAE gaps are located near the plasma edge of $\rho > 0.7$ where energetic ion drive can be neglected. The damping rates derived from the transfer function are fairly large around 10% of the eigenangularfrequency. Eigenfunctions of these TAEs calculated by AE3D indicate strong continuum damping in the plasma edge region. Electron Landau damping, collisional damping, radiative damping, and continuum damping were evaluated for the TAES, using simple analytical formulas for these damping mechanisms. Continuum damping was found to be dominant for the TAEs excited by the electrode method, because of the high magnetic shear in the edge region of a CHS plasma. However, the theoretically calculated damping rate based on a high n TAE is by a factor of 2–3 larger than the experimental results. Moreover, radiative damping is also important near the plasma edge region where magnetic shear is high and electron temperature is not very low. More accurate analysis which includes actual 3D magnetic configuration and various kinetic effects is required for quantitative comparison. This is left for future study.

ACKNOWLEDGMENTS

The authors would like to thank Dr. D. A. Spong and Professor Y. Todo for allowing us to use his numerical code AE3D and for many helpful discussions.

This work is partly supported by the Grant-in-Aid for Scientific Research from MEXT, Grant No. 16082209. One of authors (T.I.) wishes to thank to Dr. B. Peterson for his critical reading of our manuscript.

[1] A. Fasoli, C. Gormenzano, H. L. Berk, B. Breizman, S. Briguglio, D. S. Darrow, N. Gorelenkov, W. W. Heidbrink, A. Jaun, S. V. Konovalov, R. Nazikian, J.-M. Noterdaeme, S. Sharapov, K. Shinohara, D. Testa, K. Tobita, Y. Todo, G. Vlad, and F. Zonca, Nucl. Fusion **47**, S264 (2007).
[2] G. Y. Fu and J. W. Van Dam, Phys. Fluids B **1**, 1949 (1989).
[3] R. R. Mett and S. M. Mahajan, Phys. Fluids B **4**, 2885 (1992).
[4] A. Fasoli, D. Borba, G. Bosia, D. J. Campbell, J. A. Dobbing, C. Gormezano, J. Jacquinot, P. Lavanchy, J. B. Lister, P. Marmillod, J.-M. Moret, A. Santagiustina, and S. Sharapov, Phys. Rev. Lett. **75**, 645 (1995).
[5] J. A. Snipes, D. Schmittdiel, A. Fasoli, R. S. Granetz, and R. R. Parker, Plasma Phys. Controlled Fusion **46**, 611 (2004).
[6] D. Testa, A. Fasoli, and Contributors to EFDA–JET 2000 Workprogramme, Nucl. Fusion **41**, 809 (2001).
[7] J. A. Snipes, N. Basse, C. Boswell, E. Edlund, A. Fasoli, N. N. Gorelenkov, R. S. Granetz, L. Lin, Y. Lin, R. Parker, M. Porkolab, J. Sears, S. Sharapov, V. Tang, and S. Wukitch, Phys. Plasmas **12**, 056102 (2005).
[8] A. Weller, D. A. Spong, R. Jaenicke, A. Lazaros, F. P. Penningsfeld, S. Sattler, W7-AS Team, and NBI Group, Phys. Rev. Lett. **72**, 1220 (1994).
[9] M. Takechi, K. Toi, S. Takagi, G. Matsunaga, K. Ohkuni, S. Ohdachi, R. Akiyama, D. S. Darrow, A. Fujisawa, M. Gotoh, H. Idei, H. Iguchi, M. Isobe, T. Kondo, M. Kojima, S. Kubo, S. Lee, T. Minami, S. Morita, K. Matsuoka, S. Nishimura, S. Okamura, M. Osakabe, M. Sasao, M. Shimizu, C. Takahashi, K. Tanaka, and Y. Yoshimura, Phys. Rev. Lett. **83**, 312 (1999).
[10] T. Kondo, M. Isobe, M. Sasao, D. S. Darrow, K. Toi, M. Takechi, G. Matsunaga, M. Osakabe, Y. Yoshimura, C. Takahashi, S. Nishimura, S. Okamura, K. Matsuoka, and CHS Group, Nucl. Fusion **40**, 1575 (2000).
[11] K. Toi, M. Takechi, M. Isobe, N. Nakajima, M. Osakabe, S. Takagi, T. Kondo, G. Matsunaga, K. Ohkuni, M. Sasao, S. Yamamoto, S. Ohdachi, S. Sakakibara, H. Yamada, K. Y. Watanabe, D. S. Darrow, A. Fujisawa, M.Goto, K. Ida, H. Idei, H. Iguchi, S. Lee, S. Kado, S. Kubo, O. Kaneko, K. Kawahata, K. Matsuoka, T. Minami, S. Morita, O. Motojima, K. Narihara, S. Nishimura, N. Ohyabu, Y. Oka, S. Okamura, T. Ozaki, K. Sato, M. Sato, A. Shimizu, T. Shimozuma, Y. Takeiri, K. Tanaka, T. Tokuzawa, K. Tsumori, I. Yamada, Y. Yoshimura, and CHS and LHD Experimental Groups, Nucl. Fusion **40**, 1349 (2000).
[12] M. Isobe, K. Toi, H. Matsushita, K. Goto, C. Suzuki, K. Nagaoka, N. Nakajima, S. Yamamoto, S. Murakami, A. Shimizu, Y. Yoshimura, T. Akiyama, T. Minami, M. Nishiura, S. Nishimura, D.S. Darrow, D. A. Spong, K. Shinohara, M. Sasao, K. Matsuoka, S. Okamura, and CHS Team, Nucl. Fusion **46**, S918 (2006).
[13] M. Osakabe, S. Yamamoto, K. Toi, Y. Takeiri, S. Sakakibara, K. Nagaoka, K. Tanaka, K. Narihara, and LHD Experimental Group, Nucl. Fusion **46**, S911 (2006).
[14] G. Matsunaga, K. Toi, S. Kawada, J. Kotani, C. Suzuki, K. Matsuoka, and CHS Group, Phys. Rev. Lett. **94**, 225005 (2005).
[15] T. Ito, T. Kazuo, G. Matsunaga, M. Isobe, K. Nagaoka, T. Akiyama, T. Minami, and CHS Experimental Group, J. Plasma Fusion Res. **3**, 033 (2008).
[16] S. A. Cohen, J. Nucl. Mater. **76–77**, 68 (1978).
[17] T. Ito, K. Toi, G. Matsunaga, M. Isobe, T. Akiyama, T. Minami, K. Nagaoka, and CHS Experimental Group, J. Plasma Fusion Res. SERIES **8**, 1108 (2009).
[18] M. Takechi, G. Matsunaga, K. Toi, M. Isobe, T. Minami, K. Tanaka, S. Nishimura, C. Takahashi, S. Okamura, and K. Matsuoka, J. Plasma Fusion Res. **78**, 1273 (2002).
[19] K. Toi, S. Yamamoto, N. Nakajima, S. Ohdachi, S. Sakakibara, M. Osakabe, S. Murakami, K. Y. Watanabe, M. Goto, K. Kawahata, Ya. I.

Kolesnichenko, S. Masuzaki, S. Morita, K. Narihara, Y. Narushima, Y. Takeiri, K. Tanaka, T. Tokuzawa, H. Yamada, I. Yamada, K. Yamazaki, and LHD Experimental Group, Plasma Phys. Controlled Fusion **46**, S1 (2004).
[20]M. N. Rosenbluth, H. L. Berk, J. W. Van Dam, and D. M. Lindberg, Phys. Rev. Lett. **68**, 596 (1992).
[21]D. A. Spong and Y. Todo, Bull. Am. Phys. Soc. **52**, 255 (2007), Paper No. PP8.00098.
[22]H. L. Berk, J. W. Van Dam, Z. Guo, and D. M. Lindberg, Phys. Fluids B **4**, 1806 (1992).
[23]M. N. Rosenbluth, H. L. Berk, J. W. Van Dam, and D. M. Lindberg, Phys. Fluids B **4**, 2189 (1992).
[24]R. Betti and J. P. Freidberg, Phys. Fluids B **4**, 1465 (1992).
[25]N. N. Gorelenkov and S. E. Sharapov, Phys. Scr. **45**, 163 (1992).
[26]E. J. Strait, W. W. Heidbrink, A. D. Turnbull, M. S. Chu, and H. H. Duong, Nucl. Fusion **33**, 1849 (1993) (and references therein).